Nekoueian, Khadijeh; Akhoundian, Maedeh; Wester, Niklas; Laurila, Tomi

An ultra-sensitive dopamine measurement platform based on molecularly imprinted polymer-carbon hybrid nanomaterials for in vitro use

Published in:
Electrochimica Acta

DOI:
10.1016/j.electacta.2023.142029

Published: 20/03/2023

Document Version
Publisher's PDF, also known as Version of record

Electrochimica Acta 445 (2023) 142029

Contents lists available at ScienceDirect

Electrochimica Acta

journal homepage: www.journals.elsevier.com/electrochimica-acta

An ultra-sensitive dopamine measurement platform based on molecularly imprinted polymer-carbon hybrid nanomaterials for *in vitro* use

Khadijeh Nekoueian *, Maedeh Akhoundian, Niklas Wester, Tomi Laurila *

Department of Electrical Engineering and Automation, School of Electrical Engineering, Aalto University, P.O. Box 13500, Aalto 00076, Finland

ARTICLE INFO

Keywords:
Carbon-based hybrid nanomaterials
Voltammetric determination
Molecularly imprinted polymer
Dopamine
Electropolymerization

ABSTRACT

In the present study, we designed an ultrasensitive sensing platform for the evaluation of the physiologically relevant values of basal dopamine (DA) in a culture medium as a complex biological environment. The proposed sensing platform was fabricated via the integration of molecular imprinting technology with carbon hybrid nanomaterials. Carbon nanofibers (CNFs) were grown by using plasma-enhanced chemical vapor deposition (PECVD) on tetrahedral amorphous carbon (ta-C) thin films on silicon wafers. The prepared ta-C/CNFs sensing platforms were electrochemically coated with DA-imprinted polypyrrole as the molecularly imprinted polymer (MIP) or "artificial receptors". The three-dimensional MIP receptors were able to determine trace values of DA in phosphate-buffered saline solution (PBS) pH 7.4 (LOD = 5.43 nM) as well as in the absolute culture media such as DMEM/F-12 medium (LOD = 39 nM), DMEM/F-12 medium supplemented with 15% horse serum and 2.5% fetal bovine serum (LOD = 53.26 nM), and F-12 K cell culture medium (LOD = 62.57 nM), with highly physiologically relevant sensitivity and free of interference by other coexisting biomolecules and biological compounds. As all the fabrication steps of the composite electrode are compatible with common microsystem technology processes, the present results pave the way for integrating these ultra-sensitive electrodes to microelectrode arrays (MEA) platforms used for human dopaminergic neurons studies in vitro and enable continuous measurement of the basal DA concentration in real-time for instance in organoid studies.

1. Introduction

Tonic and phasic DA neurotransmission manage a wide range of essential life processes. Irregularities in tonic and phasic DA levels will lead to the emergence of potentially fatal neurological illnesses and various mental and physical disabilities (including issues in speaking, breathing, and heart function) [1].

Phasic DA release causes transient variation in extracellular DA levels, whereas tonic discharge retains absolute (basal) DA values and acts as a regulator for phasic release [2,3]. Basal DA concentrations drive fundamental neuronal functions and are influenced by both phasic and tonic neuronal activity [4]. Therefore, the development of ultra-sensitive quantification methods for the in-vitro detection of basal DA concentrations will provide the necessary insight for studying synaptic signaling, neural development, and neurodegeneration processes when working with cellular or organoid cultures. In this regard, different analysis methods have flourished to quantify the trace levels of neurotransmitters, such as spectroscopic methods [5] and the high-performance liquid chromatography-tandem mass spectrometry (HPLC-MS/MS) method [6]. However, these expensive techniques are not suitable for rapid, solvent-free, portable, on-site detection and real-time monitoring. Also, these techniques require experts to conduct measurements through a time-consuming sample preparation process and cleaning steps [2–4]. In contrast, electrochemical techniques are capable of meeting all the required parameters for the design of a highly sensitive, low-cost, rapid, portable, user-friendly, and non-invasive technique, besides their ability for miniaturization and application as a microfabricated cell culture devices or organoid-on-a-chip [7].

DA as the most important electroactive neurotransmitter can be oxidized to dopamine-o-quinone (DAQ) reversibility by using voltammetric methods, which enables screening of its levels in biological media by using electrochemical techniques. The success of electrochemical techniques in measuring DA or any other similar target molecule is crucially dependent on the physicochemical and morphological properties of the electrode material used.

Modification of electrode materials and the application of various forms of bio-based receptors on the surface of the sensing platform as biorecognition elements, such as enzymes (tyrosinase or polyphenol

* Corresponding authors.
E-mail addresses: Khadijeh.Nekoueian@aalto.fi (K. Nekoueian), Tomi.Laurila@aalto.fi (T. Laurila).

https://doi.org/10.1016/j.electacta.2023.142029
Received 26 August 2022; Received in revised form 9 February 2023; Accepted 9 February 2023
Available online 12 February 2023

oxidase) and DNA in aptamers [8] have been considered as solutions for gaining adequate selectivity in the presence of conventional coexisting electroactive biomolecules. But the absence of sufficient sensitivity due to lack of conductivity and electrocatalytic activity besides low chemical and thermal stability has restricted the use of these biorecognition elements in the design of sensors [9].

Molecular imprinting technology allows us to biomimic artificial receptors and the basic functions of neurotransmitter receptors in living systems on the surface of a sensing platform. MIPs are cost-effective alternatives to natural receptors. Furthermore, MIPs have demonstrated high sensitivity and durability as "artificial antibodies" for selective interaction and recognition with a target neurotransmitter.

Among various functional conducting monomers, pyrrole has been employed significantly as a functional monomer for imprinting DA as a template in the fabrication of MIP-based biosensors for DA sensing due to its excellent electrochemical features such as ease of polymerization, biocompatibility, low impedance, and high charge storage capacity [9–11].

In view of these advantages, polypyrrole (PPy)-based materials have been significantly investigated in the design of DA sensors, particularly when the development of an anti-interference layer is demanded. The electrochemical fabrication of a PPy layer on the surface of a glassy carbon electrode doped with sulfonated-cyclodextrin was described by Harley et al. [12]. This DA sensor had a sensitivity of 0.90 μA μM^{-1} and a detection limit of 1.0 μM. The anti-interference characteristic of this electrode was attributed to a weak inclusion complex between DA and cyclodextrins [12]. Eom et al. designed a PPy-based sensor for DA detection by integrating PPy with sodium dodecyl sulfate (SDS) and a multi-walled carbon nanotube (PPy/SDS/MWCNT) electrode. This PPy/SDS-MWCNT electrode displayed good sensitivity toward DA in the presence of common interfering biomolecules including ascorbic acid (AA) and glucose (Glc), and the limit of detection was determined to be 136 pM [13]. Novosad et al. developed an AA anti-interference platform by electro-polymerizing thin layers of PPy in the presence of cyclopentenedione monomers. The calculated detection limit was 10.0 nM and the selectivity ratio DA/AA was 1:260 [14]. According to recent reports, the efficiency of surface-modified electrodes using PPy-based nanomaterials for DA detection is evident. However, imprinting specific molecular recognition sites on the PPy layer has been considered an elegant technique to develop ultra-sensitive DA biosensors [15–19]. Mauche et al. developed DA-imprinted PPy films for electrochemical picomolar DA detection. The dopamine-imprinted PPy films were shown to be highly selective for DA against interferents such as AA, 2-phenyl ethylamine (PEA), and noradrenaline (NAD), with a limit of detection as low as 5.7 pmol L^{-1} [19]. Slimi et al. used electropolymerized over-oxidized PPy (OPPy) on a glassy carbon electrode for imprinting DA. The prosed MIP-based electrode detected DA with a detection limit of 10 pmol L^{-1}. Li et al. developed another ultra-sensitive MIP-based sensor by integrating CNTs on graphene foam (GF/CNT) for indirect detection of DA by using a redox probe. The GF/CNT/MIP electrode displayed an ultralow detection limit of 0.000667 pmol L^{-1}, and good selectivity [20].

The modification of the DA imprinted PPy with various nanomaterials ranging from metal nanoparticles [21,22] to carbon nanostructured [18–21,23] has been considered an elegant technique to enlarge the sensing surface area for forming more accessible recognition receptors and facilitating charge transport between the sensing platform and target media [24]. Carbon-based nanostructures have demonstrated outstanding properties such as high conductivity, high biocompatibility, inert nature, and excellent mechanical and thermal stability, which make them efficient electron mediators and reliable immobilizing platforms in the modification of MIP-based biosensors for sensing DA [25].

Most of the reported DA imprinted PPy-carbon nanostructured composites have been designed using PPy/CNTs composites [20,26,27] and PPy/graphene composites [18,27–29] and mostly were used in phosphate buffer solution (PB) as electrolyte for measurement of DA (Table 2). Here, for the first time, we designed a novel DA imprinted PPy/carbon hybrid nanomaterial/silicon-based sensing platform capable of measuring DA in culture medium as a complex electrolyte without sacrificing sensitivity. This novel carbon hybrid material was fabricated by growing CNFs on top of ta-C thin films on a silicon substrate using a nickel catalyst and Ti adhesion layer [30]. The combination of the properties of ta-C (as an antibacterial and biocompatible material) and CNFs (as a highly conductive and electrocatalytic nanomaterial) results in a highly qualified and biocompatible carbon-based sensing platform. The prepared ta-C/CNFs sensing platform demonstrated a wider and more stable water window compared to the ta-C [31] as well as high resistance toward electrode surface fouling by biological media components and DA oxidation byproducts [32]. The employment of DA imprinted PPy as MIP on the ta-C/CNFs sensing platform led to the establishment of a highly sensitive DA sensing platform by considering the advantages of MIPs and carbon hybrid nanomaterials. The designed MIP/ta-C/CNFs sensing platform was successfully used for in vitro determination of the basal DA levels with physiologically relevant sensitivity in cell culture medium independently of fouling or interference by other coexistence biomolecules and compounds in the medium. We believe that (i) these materials are compatible with microsystem technologies, (ii) thus can be used to fabricate MEAs and other similar devices that (iii) enable continuous monitoring of basal level DA in cell and organoid studies.

2. Experimental

2.1. Materials

Gibco F-12 K Nut Mix (Nutrient Mixture Kaighn's Modification) Medium and Gibco™ DMEM/F-12, Gibco™ Horse Serum (HS) (New Zealand origin), and Gibco Fetal Bovine Serum (FBS) were supplied from Thermo Fisher Scientific. Pyrrole, 98+% was purchased from Alfa Aesar. All other chemicals were analytical reagent grade from Merck. All aqueous solutions were prepared with doubly distilled deionized water.

The 1 M PBS solution was prepared by mixing 8 g of NaCl, 0.2 g of KCl, 1.44 g of Na_2HPO_4, and 0.24 g of KH_2PO_4 in 800 mL of distilled water. The pH of the solution was maintained at 7.4 using a 1 M HCl or NaOH solution.

2.2. Instruments

Cyclic voltammetry (CV) and differential pulse voltammetry (DPV) measurements were conducted using a Gamry potentiostat (Reference 600) coupling with a conventional three-electrode system including a working electrode, a saturated Ag/AgCl reference electrode, and a Pt wire as the counter electrode. A silver wire coated with AgCl was used as a reference electrode for the electrodeposition of PPy on the surface of ta-C/CNFs electrodes and for conducting the measurements in biological media.

Voltammetric experiments were carried out in PBS (pH 7.4; 0.1 M). The potentiostat was used to test the contact resistance of the fabricated working electrodes to ensure proper contact and to show that there are no significant differences in resistance among the different working electrodes. All solutions were deoxygenated by purging the pure nitrogen for 30 min before conducting measurements. After fabrication of MIP, the DA molecules entrapped as templates were removed/washed, and then the washed ta-C/CNFs/MIP electrode was used for DA analysis. The absence of DA molecules in the washed ta-C/CNFs/MIP electrodes was checked by running DPV in fresh PBS 7.4. The electrodes were ready for use when no DA signal was detected by the DPV. The washed ta-C/CNFs/MIP electrodes were used only for one measurement, and the washing procedure wasn't employed to reuse the ta-C/CNFs/MIP electrode during the analysis. A washed ta-C/CNFs/MIP electrode was placed in a voltammetric cell containing the desired concentration of DA in PBS pH 7.4 or culture medium for 10 min before recording the

response signal by DPV or CV.

A digital pH/mV/ion meter (JENWAY) was applied for the preparation of the buffer solutions and adjusting the pH of the supporting electrolytes at 7.4 (by using a 1 M HCl or NaOH solution), in electrochemical measurements.

The surface morphology of ta-C, ta-C/CNFs, and ta-C/CNFs/MIP were studied by scanning electron microscope (SEM) (Zeiss Sigma VP). Micro-Raman spectroscope (WITec Alpha 300 RA+) equipped with an optical microscope was used for Raman spectroscopy at a laser excitation wavelength of 532 nm employing a 50 × objective lens. The Raman data were fitted with Lorentzian curves.

2.3. Material fabrication

2.3.1. ta-C fabrication

Direct current-magnetron sputtering (DCMS) was used to establish a 20 nm thick Ti layer on the surface of a highly conductive (0.0010.002 cm) p-type Si wafer (Utrasil). The ta-C layer was deposited on top of the Ti adhesion layer using a filtered cathodic vacuum arc (FCVA) without breaking the vacuum in between. Then, for DCMS, a 2-in Ti target (Kurt J. Lesker Company) was set at a deposition distance of 220 mm from the sample. A discharge power of 100 W, a total pressure of 0.67 Pa, and an Ar gas flow rate of 29 sccm were used throughout the deposition. FCVA was installed with two graphite cathodes in a dual cathode design (6.35 mm diameter, 99.95% purity, Goodfellow). A 2.6 mF capacitor bank was charged to 400 V while keeping an arc current of 0.7 kA and a pulse width of 6 ms. The overall pressure was kept below 104 Pa during the deposition [33].

2.3.2. ta-C/CNFs fabrication

Plasma-enhanced chemical vapor deposition (CVD) was used to form CNFs on ta-C. A 10 nm thick Ni layer was deposited on the ta-C surface using cathodic arc deposition. In a cold-wall CVD reactor with a chamber pressure of 102 mbar, the catalyst-coated ta-C wafers were annealed for 3 min at 400 °C. The chamber was heated to 400 °Celsius at a rate of 250° per min. Following the annealing stage, the chamber pressure was raised to 0.1 m bar, and the chamber was filled with NH_3 buffer (100 sccm). The temperature of the chamber was then raised to 750 °C at a rate of 300 °C per minute. After reaching 675 °C, a 150 W DC plasma was generated in the chamber by introducing a carbon precursor, C_2H_2 (30 sccm), and raising the NH_3 flow to 125 sccm. The growth phase lasted 10 min, resulting in fibers that were vertically oriented [34].

2.4. Electrode preparation

The ta-C and ta-C/CNFs/silicon-based samples were used to prepare working electrodes. In this regard, their backsides were scratched by using a diamond and copper palette and connected to a copper FR4-PBB body. A protective coverage of polytetrafluoroethylene (PTFE) tape with a 3 mm diameter hole (applied electrode surface area) was used to sandwich the sample and copper sheet.

2.4.1. Fabrication of MIP (DA imprinted PPy) on ta-C/CNFs and NIP (non-imprinted PPy) on ta-C/CNFs

Under the optimized conditions, pyrrole as the functional monomer and DA as the template molecule were electro-polymerized on the surface of the ta-C/CNFs electrode to create a MIP layer. This was carried out without the need for any additional reagents such as enzymes or mediators. Briefly, the ta-C/CNFs electrode was placed in a freshly prepared and degassed 1 M PBS (pH 6.0) containing 10.0 mM pyrrole and 2.0 mM DA (the molar ratio was 5:1). The CV method was employed to electropolymerize MIP on the surface of ta-C/CNFs at a scan rate of 100 mV s^{-1} in the potential range of -0.2–0.8 V. The number of employed cycles was 10. The first scan demonstrated redox signal peaks of DA, which were gradually reduced at higher cycles because of the formation of the MIP layer on the electrode surface (Fig. 1).

The effect of supporting electrolyte pH in the electrodeposition step was studied. It was seen that the signal value increased from pH 3.0 to 6.0, whereas it decreased at higher pHs. The highest peak current was obtained at pH 6.0. Thus, we used pH 6.0 for the electrodeposition of MIP on the ta-C/CNFs platform. In neutral or alkaline PBS, DA polymerizes into a polydopamine layer on the electrode's surface and restricts the charge transport process [35,36]. The inserted DA molecules were removed from the polymeric structure in two steps: chemical washing and electrochemical washing. The chemical template removal step involved immersing the ta-C/CNFs/MIP electrode in a deionized water-ethanol solution (1:1, v/v) for 15 min. The subsequent electrochemical template removal step was carried out using the CV method in 1 M PBS (pH 6.0) in the potential range of -0.2–0.6 V (scan rate: 10 mVs^{-1}) and was continued until the DA redox peaks vanished. The absence of DA in washed ta-C/CNFs/MIP electrode was checked by running DPV in fresh PBS 7.4. The obtained ta-C/CNFs/MIP was employed in subsequent studies under optimal settings. In the absence of DA, the same method was used to create NIP on the surface of the ta-C/CNFs electrode. The fabricated MIP and NIP electrodes can be stored at room temperature in a 0.1 M PBS pH 7.4 solution [28].

2.5. Voltammetric DA detection

The obtained ta-C/CNFs/MIP electrodes were incubated in the desired concentration of DA solution (0.1 M PBS pH 7.4) for 10 min for conducting voltammetric experiments. The same detection model was adopted for the ta-C/CNFs/NIP electrode and the ta-C/CNFs/MIP electrode for DA measurement in biological media (F-12 K Gibco Nut Mix,); and DMEM/F-12 with 2.5% FBS, 15% HS.

3. Results and discussion

3.1. Structural characterization

Scanning electron microscopy (SEM) was used to study the surface morphology of ta-C, ta-C/CNFs, and ta-C/CNFs/MIP electrodes. The growth of forest-like CNFs on the surface of ta-C is obvious by comparison of SEM images of ta-C (Fig. 2A) with ta-C/CNFs (Fig. 2B and C). The length of the CNFs on the surface of ta-C was measured to be approximately 2.5 μm, which is in agreement with previous results

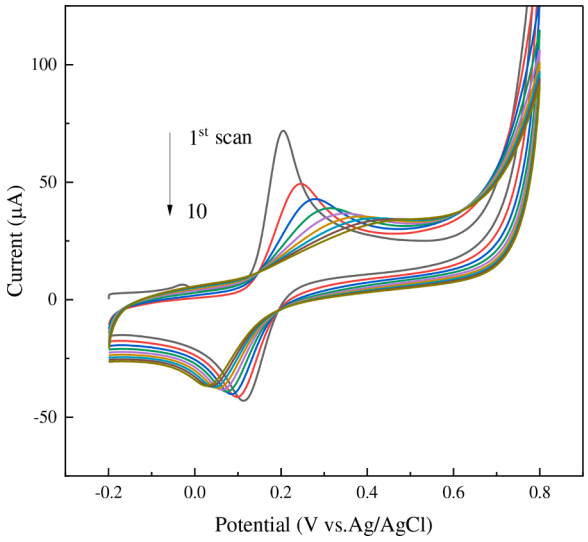

Fig. 1. Electrochemical imprinting of DA on the ta-C/CNFs electrode using the CV technique in the potential range of -0.2–0.8 V for 10 cycles with a scan rate of 100 mV s^{-1} in a 1.0 M PBS (pH 6.0) including 10.0 mM pyrrole and 2.0 mM DA.

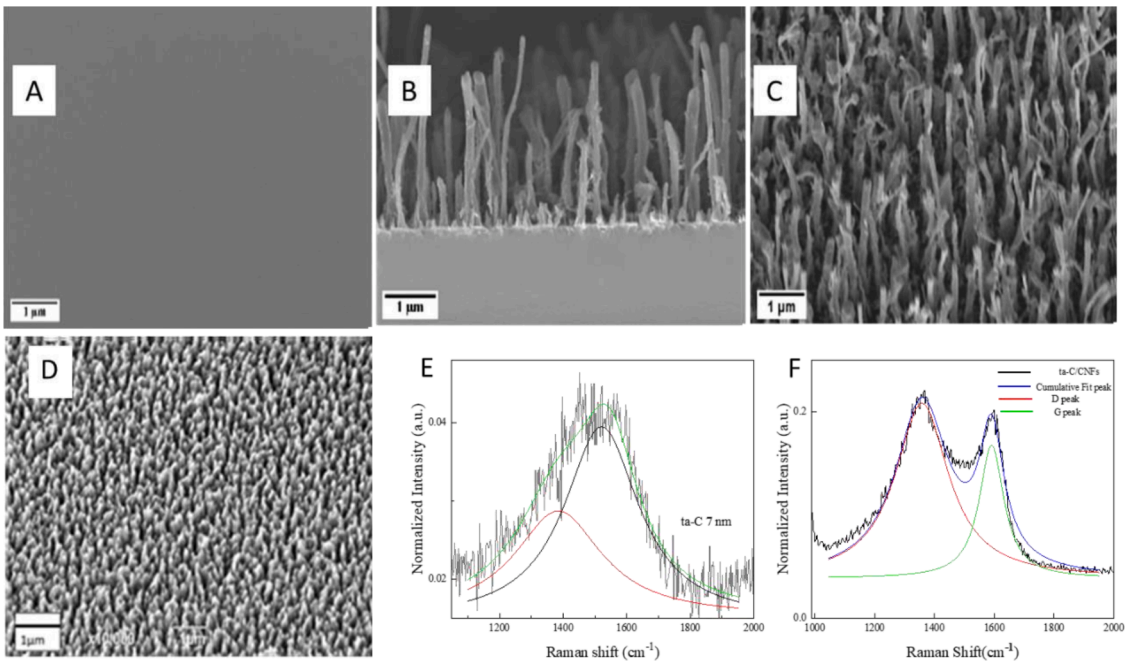

Fig. 2. SEM micrographs showing ta-C (A), the CNFs grown on top of ta-C layer (B), and ta-C/CNFs cross-section 25° angle view (C); SEM images of ta-C/CNFs/MIP (D); Raman spectra of ta-C (E) and ta-C/CNFs (F).

(Fig. 2B) [34]. Figs. 2D and S1 show SEM images of ta-C/CNFs/MIP, indicating uniform electropolymerizing of pyrrole on CNFs (more detailed images are in Fig. S2).

The Raman spectra demonstrated two peaks at 1366 (D band relating to the disordered structure of carbon atoms), and at 1587 cm^{-1} (G band resulting from sp^2 carbon atoms in olefinic chains). The D band was lower and wider at ta-C than it was at ta-C/CNFs (Fig. 2E and F). The ratio of the intensity of these two bands(I_D/I_G ratio) is used to display the value of defects in the carbon-based materials. The I_D/I_G values were calculated to be 0.6 for ta-C [37], which increased to the amount of 1.33 at ta-C/CNF (evaluated based on the Lorentzian function fit). It can be deduced that the higher quantity of defects in the ta-C/CNFs as well as their forest-like structure can provide more effective contact with the electrolyte for charge accumulation and facile charge transport [38]. Furthermore, electrochemical studies firmly validated the precedence of ta-C/CNFs over ta-C.

3.2. Electrochemical characterization of the modified electrodes

The electrochemical performance of ta-C/CNFs/MIP, ta-C/CNFs/NIP, ta-C/CNFs, and ta-C electrodes were studied by using CV in presence of 5 mM $Ru(NH_3)_6^{2+/3+}$ in 1 M KCl solution as an outer-sphere redox probe (OSR) (Fig. 3A). Generally, OSR probes react with electrode free of any specific chemical/electrocatalytic interactions or sensitivity toward electrode surface chemistry. No significant differences were observed between various electrodes by OSR (electrochemical parameters presented in Table S1). Furthermore, the electrodeposition of PPy on ta-C/CNFs under optimized parameters did not decrease the performance of CNFs at ta-C/CNFs/MIP and ta-C/CNFs/NIP electrodes. The heterogeneous charge-transfer rate constants (k^0) at ta-C, ta-C/CNFs, ta-C/CNFs/NIP, and ta-C/CNFs/MIP were calculated by using the Nicholson method respecting values of ΔE_p [27]. The quantity of k^0 is characteristic of a particular electrochemical system, which involves the form of electrode material where the reaction takes place. As a result, it is a crucial electrochemical characteristic for directly contrasting

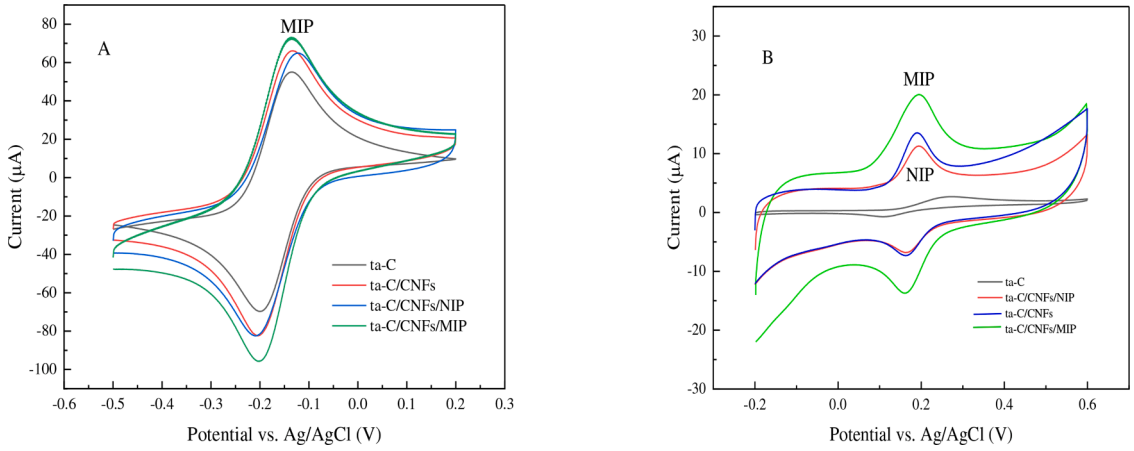

Fig. 3. CVs of ta-C/CNFs/MIP, ta-C/CNFs/NIP, ta-C/CNFs, and ta-C electrodes in 5 mM $Ru(NH_3)_6^{2+/3+}$ in 1 M KCl (A); and 100 µM DA in 0.1 M PBS pH 7.4 (after being incubated for 10 min) (B). The scan rate was 100 mVs^{-1}.

various electrode materials. The fact that the peak potentials were close to each other at ta-C/CNFs, ta-C/CNFs/NIP, and ta-C/CNFs/MIP proved that there was no change in charge transfer kinetics. In this situation, we assumed that the density of states at the electrode's surface was equal. The obtained results are consistent with our previous studies [39].

The electrochemical performance of ta-C/CNFs/MIP in the presence of DA (100 μM) as an imprinted template as well as inner sphere redox prob (ISR) was investigated and compared to ta-C/CNFs/NIP, ta-C/CNFs, and ta-C electrodes in 0.1 M PBS pH 7.4. The specific chemical interactions between the electrode surface and the redox species have a strong influence on inner-sphere redox reactions. Adsorption is the most common mechanism that occurs, and it can result in either an amplified (electrocatalytic) or limited redox process. It is generally known that ISR systems are sensitive to electrode surface chemistry [40]. As a result, different outcomes are expected in comparison to the OSR system. In Fig. 3B, CNFs and ta-C electrodes demonstrated different electrochemical behavior in presence of DA due to clear differences in their surface chemistry as well as their physicochemical properties. Amorphous structures of ta-C (metal catalysts free) with sp^3 bonded carbon in their bulk regime (higher sp^3 content) demonstrated slower kinetics and an increase in $\triangle E_p$ compared to CNFs [39]. On other hand, the structure of CNFs is predominately crystalline with a higher amount of edge plane sites, which leads to a higher content of oxygen functional groups at its surface. Oxygen functional groups can facilitate proton tunneling. Furthermore, the existence of residual metal catalysts (Fe particles) in the structure of CNFs led to enhanced kinetics (by catalyzing the redox reaction) and a significantly lower $\triangle E_p$ in presence of DA (more detailed physicochemical and electrochemical studies on ta-C and CNFs are available in our recent work [39]) (Table S2).

Furthermore, the presence of nano-sized imprinted recognition sites at ta-C/CNFs/MIP that were of the same size and shape as DA molecules resulted in a higher redox response signal compared to the non-imprinted PPy at ta-C/CNFs/NIP (Fig. 3B). These findings proved the efficiency of the designed ta-C/CNFs/MIP sensing platform for DA detection. It is crucial to emphasize that there is no relationship between the electrochemical results for the OSR probe and the electrochemical performance of electrodes in the presence of DA (ta-C/CNFs, ta-C/CNFs/NIP, ta-C/CNFs/MIP, and ta-C). Because the OSR system is a pure electron transport mechanism that relates to the electronic architecture of the working electrode material, whereas the ISR system is an ion transport process that is greatly impacted by surface chemistry [39].

The coexistence of high concentrations of AA and (uric acid) UA in biological fluids and overlaps of their oxidation peaks with DA is known as the key problem in DA detections, which has been studied significantly. Here, the performance of ta-C/CNFs/MIP toward detecting DA in the presence of AA and UA was studied and compared with ta-C/CNFs/NIP, ta-C/CNFs, and ta-C electrodes by using DPV in 0.1 M PBS pH 7.4 containing 10 μM DA, 1 mM AA, and 200 μM UA (Fig. 4). The oxidation peaks of AA, DA, and UA overlapped at the ta-C electrode. Modification of ta-C with CNFs had a great effect on the amplification of response signals. However, the oxidation peaks of AA and DA still overlapped at this electrode. Electrodeposition of the PPy layer on the surface of CNFs led to well-distinguished response signals for AA, DA, and UA without any overlapping. The ta-C/CNFs/MIP electrode demonstrated good selectivity toward detecting DA in presence of AA. However, the oxidation peak of UA was well-defined at ta-C/CNFs/MIP without overlapping with the DA response signal. These results illustrated the favorable sensing performance of the ta-C/CNFs/MIP arising from the nano-sized template cavities (recognition sites). The performance of ta-C/CNFs/MIP was studied in DA (10.0 μM) solution in the presence of potential inferring species such as serotonin (SR, 1.0 μM) and 3,4-dihydroxyphenylacetic acid (DOPAC) (10.0 μM). The changes in the current signal were as low as ±5.5% demonstrating the efficiency of the ta-C/CNFs/MIP for use in complex media.

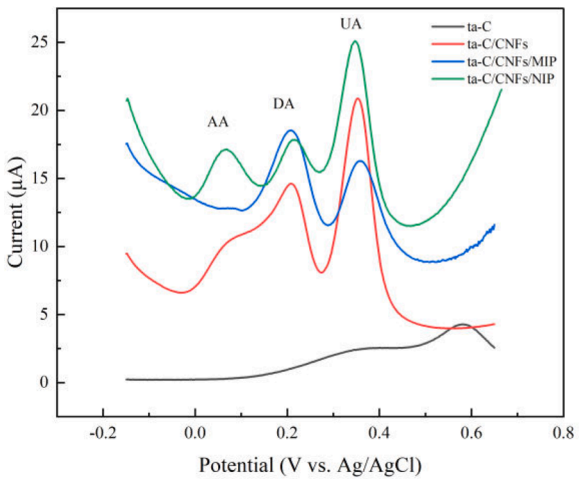

Fig. 4. DPVs of 10 μM DA in the presence of 1 mM AA, and 200 μM UA at ta-C, ta-C/CNFs, ta-C/CNFs/NIP, and ta-C/CNFs/MIP electrodes in 0.1 M PBS pH 7.4 under optimized condition. Pulse time: 0.05 s, pulse amplitude: 50 mV, electrode area was 0.07 cm^2.

3.3. Optimization results

The effects of various parameters, including (i) the molar ratio of functional monomers to template molecule, (ii) the number of electropolymerization cycles and thickness of the MIP layer, and (iii) incubation time, were studied and optimized to improve electrochemical behavior of the ta-C/CNFs/MIP for DA sensing (Table 1). The effect of different molar ratios of functional monomer (pyrrole) to template molecules (DA as target analyte) from 1:1 to 9:1, on the oxidation peak current of (10 μM) DA in 0.1 M PBS (pH 7.4) was examined. The number of imprinted recognition sites at ta-C/CNFs/MIP was boosted by increasing the number of functional monomers for binding to additional DA molecules from 1:1 to 5:1 (Fig. 5A). Peak current decreased at higher ratios due to a reduction in the number of template molecules involved in the creation of recognition sites [23]. The effect of the number of electropolymerized cycles and thickness of the MIP layer on improving the electrochemical performance of ta-C/CNFs/MIP toward detecting DA was studied by increasing the number of cycles from 5 to 20. The best response signal was obtained at 10, which may be attributed to the development of additional recognition sites at ta-C/CNFs/MIP for sensing DA (Fig. 5B). Excessive development of the MIP layer resulted in a significant decrease in the response signal besides more difficulty in removing the imprinted template from the polymeric structure. This phenomenon can be related to the electrodeposition of PPy between the CNFs gaps and the formation of flat islands on CNFs (Figs. 5D and S2), resulting in a decrease in the contact surface area between the electrode and the electrolyte. This finding is consistent with the recent literature [41]. The influence of different incubation times (60, 300, 600, 900, and 1200s) on the oxidation peak current of DA in 0.1 PBS solution pH 7.4 was studied at ta-C/CNFs/MIP (under optimized conditions). The highest peak current was obtained at 600 s, demonstrating the high suitability of ta-C/CNFs/MIP in fast DA sensing. By increasing time, the

Table 1
Optimized parameters at ta-C/CNFs/MIP.

Optimization parameters	Study target	Optimized results
Monomer to template ratio	The number of effective recognition sites	5:1
The number of electro-polymerization cycles (MIP layer thickness)	Accessibility of recognition sites Ease of template removal step	n: 10
Incubation time	DA extraction rate	600 s

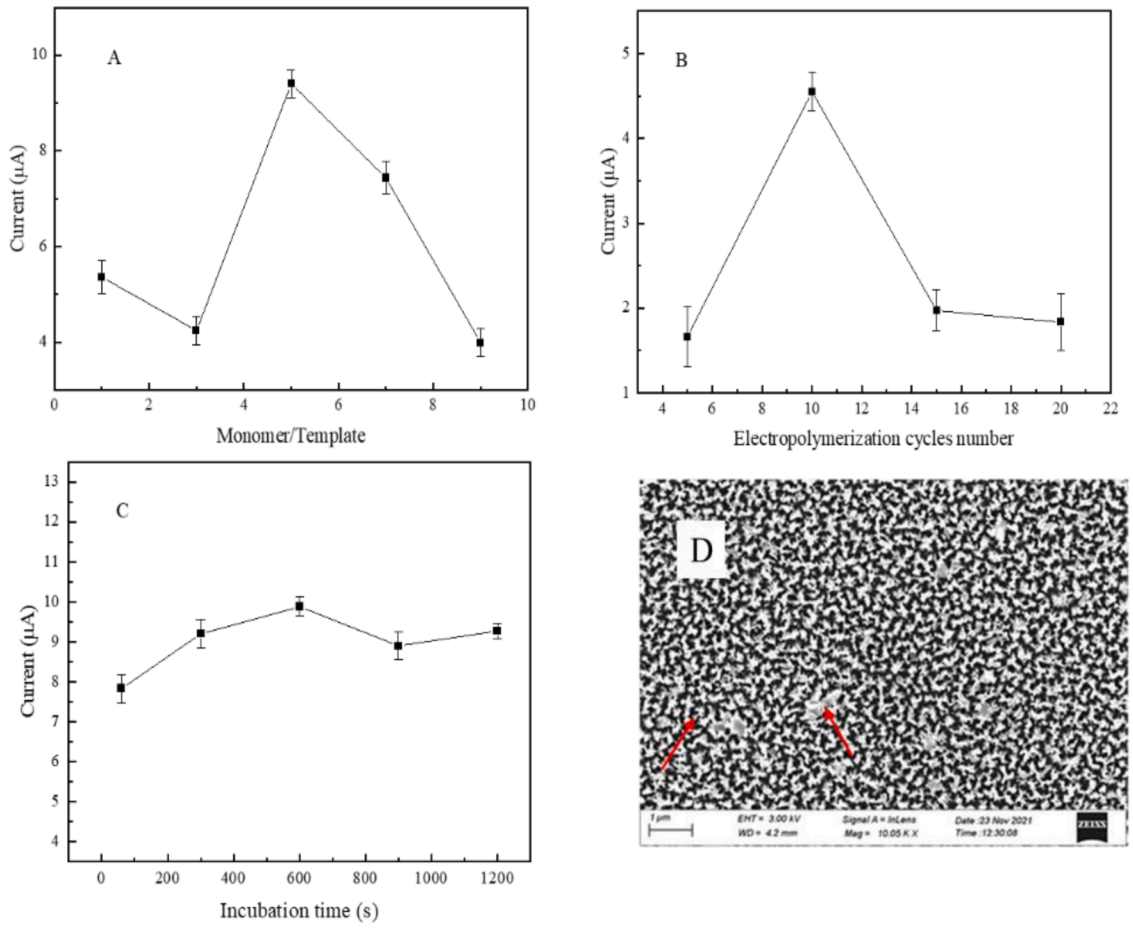

Fig. 5. Optimization of different parameters: The effects of the ratio of functional monomers (PPy) to template molecules (DA) (1:1, 3:1, 5:1, 7:1, 9:1) (A); electropolymerization cycles number (cycles number were 5, 10, 15, and 20) (B); incubation time (60, 300, 600, 900 and 1200s) (C), on the response signal of the 10.0 μM DA in 0.1 M PBS (pH 7.4) at ta-C/CNFs/MIP electrode; SEM image of established PPy flat islands (islands were marked with red arrows) on the surface of the ta-C/CNFs/MIP electrode in a higher number of electro-polymerization cycles (D).

current of the response signal decreased slightly and remained steady for 10 min. It can be suggested that DA molecules occupied most of the active recognition sites on the surface of ta-C/CNFs/MIP [21] (Fig. 5C).

The effect of CV scan rate (ν) on the redox peak current of DA at the ta-C/CNFs/MIP was also studied (Fig. 6A). The I_{pa} and I_{pc} were enhanced by increasing the scan rate (from 10 to 450 mVs^{-1}). The linear relationship between I_p and ν suggested an adsorption-controlled mechanism for DA oxidation/reduction on the ta-C/CNFs/MIP. The following equations were obtained for I_{pa} and I_{pc} versus ν (Fig. 6B).

$$I_{p,a}\ \mu A = 1.75 + (0.219\ \nu / (mVs^{-1})), (R^2 = 0.990) \quad (1)$$

$$I_{p,c}/\mu A = 0.86 - (0.123\ \nu/(mVs^{-1})), (R^2 = 0.984) \quad (2)$$

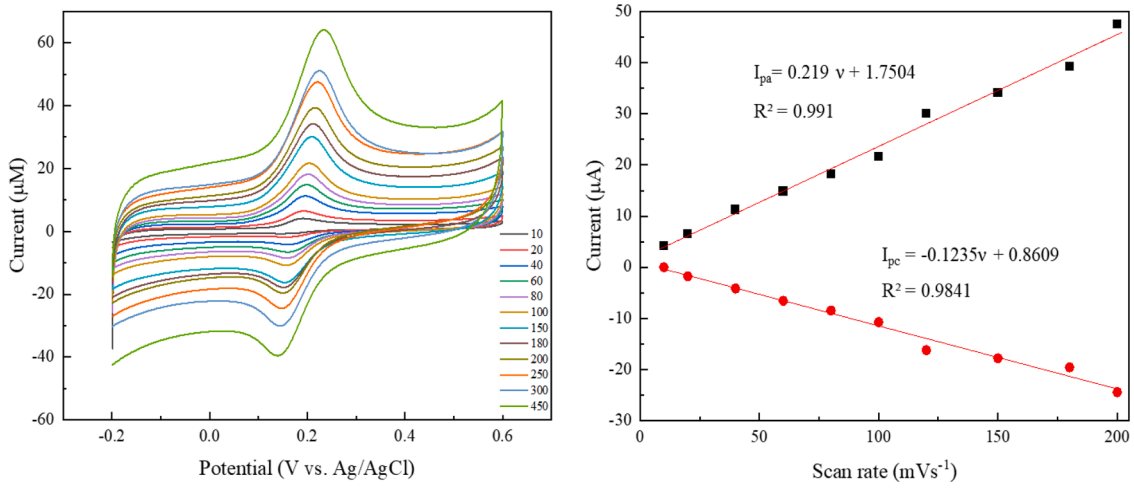

Fig. 6. Cyclic voltammograms of the 100.0 μM DA in 0.1 M PBS (pH 7.4) at ta-C/CNFs/MIP electrode in various ν (10, 20, 40, 60, 80, 100, 150, 180, 200, 250, 300 and 450 mVs^{-1}) (A); Plots of the anodic and cathodic peak currents vs. different ν with fits of lines to these data (B).

3.4. Analytical results

The analytical performance of the ta-C/CNFs/MIP electrode toward different concentrations of DA (0.0, 10, 100, 250, 500, 1, 2.5, 5 and 10 μM) was evaluated by using DPV as it provides higher sensitivity than CV. DPV measurements were conducted under the optimized conditions in 0.1 M PBS pH 7.4 as a supporting electrolyte (Fig. 7A). The response signal was enhanced by increasing DA concentration. The recorded peak currents were linearly proportional to the DA concentration in the range of 10.0 nM to 10 μM with a slope of 0.502 μA/μM and a correlation coefficient (R^2) of 0.998. The limit of detection was calculated to be 5.43 nM (Fig. 7B), which is 100 times better compared to ta-C/CNFs with LOD of 500 nM (studied in our group previously [31]), which revealed the role of MIP in amplifying the sensitivity of ta-C/CNFs.

Furthermore, the performance of ta-C/CNFs/MIP in sensing basal DA concentration was evaluated in absolute culture media such as DMEM/F-12 medium, DMEM/F-12 medium supplemented with 15% HS and 2.5% FBS (for dopaminergic neurons cells and glial cells), and F-12 K cell culture medium, which are rich in amino acids and vitamins, glucose (1 g/L), and sodium pyruvate [14,15].

The results demonstrated a linear relationship between the response signal and basal DA concentration in a linear range of 50.0–1.0 μM. The detection limits for DMEM/F-12 medium and DMEM/F-12 medium supplemented with 15% HS and 2.5% FBS, and F-12 K medium were evaluated to be 39 nM (Fig. 8A), 53.26 nM (Fig. 8B), and 62.57 nM (Fig. 8C), respectively. According to our recent work [21], the loss of sensitivity and fouling in complex matrixes was thought to be a limit for the use of carbon-based electrodes in culture media, but this was significantly recovered at the proposed MIP/ta-C/CNFs sensing platform. It should be highlighted that the larger standard deviation of the blank signals in culture media compared to PBS led to higher detection limit values (Table 2). This study demonstrated that the designed MIP/ta-C/CNFs sensing platform can be successfully used for in vitro determination of the basal DA levels with physiologically relevant sensitivity in PBS (pH 7.4) as well as basal culture medium as a complex environment independently of interference by other coexistence compounds and active biomolecules (Fig. 4).

The obtained results were compared with some previous DA imprinted PPy/carbon-based sensors in Table 2. Most of the reported MIP/carbon-based sensors were employed in PB solution as an electrolyte and not used in PBS pH 7.4 or culture medium. Our designed ta-C/CNFs/MIP electrode demonstrated high sensitivity to detect DA in physiologically relevant pH 7.4 in PBS, and more importantly in a complex basal culture medium in a wide dynamic linear range with an excellent limit of detection. Furthermore, the notable advantage of the proposed ultra-sensitive electrode is its capability to be processed (integrated) into MEA structures to make devices, which is not the case with some graphene aerogels (Table 2). Taken together, we can conclude that the proposed ta-C/CNFs/MIP is an ultra-sensitive sensing platform toward basal DA, even in complex physiological media *in vitro*, besides its potential for application as a microfabricated cell culture device or neuron sys-on-a-chip.

4. Conclusion

In the present study, we proposed an ultra-sensitive MIP-based sensing platform by the integration of molecularly imprinting technology and carbon-based hybrid nanomaterial advantages. We designed the ta-C/CNFs sensing platform successfully by growing vertically forest-like CNFs on the top of ta-C/silicon wafers by using plasma-enhanced chemical vapor deposition. The SEM and Raman spectra demonstrated that the ta-C/CNFs sample has a forest-like structure and is defective. Also, electrochemical studies confirmed the high performance of ta-C/CNFs compared to ta-C. Thus, the fabricated carbon hybrid material (ta-C/CNFs) on silicon wafers was used as an effective substrate for the design of an ultrasensitive MIP-based carbon hybrid sensing platform. All electrode fabrication steps were optimized toward the detection of DA with physiologically relevant sensitivity in PBS (pH 7.4). Electrochemical studies revealed the high performance of the ta-C/CNFs/MIP electrode for the detection of low levels of basal DA in the linear range of 10.0–10.0 μM. The limit of detection was calculated to be 5.43 nM in PBS pH 7.4, which is a highly physiologically relevant sensitivity for *in vitro* studies. Furthermore, the efficiency of ta-C/CNFs/MIP for sensing DA was investigated in a basal culture media, which is full of various biological compounds such as amino acids and vitamins, glucose (1 g/L), sodium pyruvate, 15% HS, and 2.5% FBS. Obtained results demonstrated a linear relationship between response signal and basal DA concentration in the sub-micromolar zone, revealing the excellence of the designed sensing platform for sensitive detection of basal values of DA in a complex environment with high sensitivity for the first time. Moreover, as all the process steps of the ta-C/CNFs/MIP sensing platform are compatible with common microsystem technology processes, the proposed platform is capable of being integrated into MEA and applied in microfabricated cell culture devices as a smart cell culturing substrate or neuron system-on-a-chip for the real-time monitoring of basal DA levels as an indicator for tracking the activity of dopaminergic

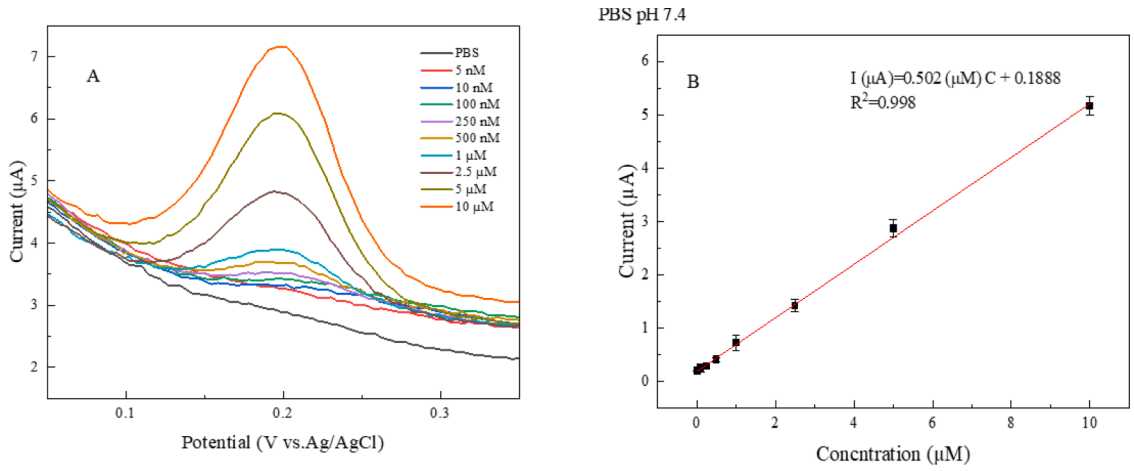

Fig. 7. DPV signals for different concentrations of DA (0.0, 10 nM, 100 nM, 250 nM, 500 nM, 1 μM, 2.5 μM, 5 μM, 10 μM) at ta-C/CNFs/MIP electrode in 0.1 M PBS pH 7.4 (A); The corresponding calibration plot for the ta-C/CNFs/MIP electrode in 0.1 M PBS pH 7.4 under optimized conditions ($n = 3$) (B). The incubation time was 10 min. The pulse time was 0.05 s, the pulse size was 50 mV, and the electrode area was 0.07 cm^2.

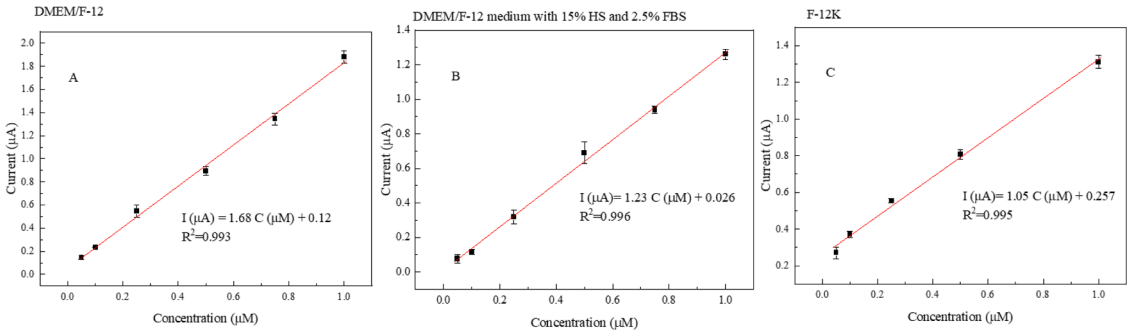

Fig. 8. Calibration plot for the ta-C/CNFs/MIP electrode at different concentrations of DA (50, 100, 250, 500, 750 and 1 μM) in DMEM/F-12 medium ($n = 3$) (A); In DMEM/F-12 medium supplemented with 15% HS and 2.5% FBS ($n = 5$) (B); And in F-12 K medium under optimized conditions ($n = 3$) (C). The incubation time was 10 min. The pulse time was 0.05 s, the pulse size was 50 mV, and the electrode area was 0.07 cm^2.

Table 2
Comparison of the previous MIP/carbon-based sensors for DA detection.

Electrode's material	Linear range (μM)	Electrolyte	The detection limit (nM)	Refs.
DA imprinted PPy /MWCNT/GAs [a]	0.005–20.0	PB (pH:6)	1.67	[28]
DA imprinted PPy - o-PD [b]		PBS (pH:6)	3972	[42]
DA imprinted PPy/ /pThi/ NPG [c]	3–100	PB (pH:7)	100	[29]
DA imprinted poly(p-ATP) [d]	0.05–0.2	PBS (pH:7.4)	18	[43]
DA imprinted poly(AHQ) /GR [e]	0.1–1.4	PB (pH:7)	32	[29]
DA imprinted PPy -ta-C/CNFs	0.01–10	PBS (pH 7.4)	5.4	This work
DA imprinted PPy -ta-C/CNFs	0.01–1	F-12K	62.57	This work
DA imprinted PPy -ta-C/CNFs	0.01–1	DMEM/F-12	39	This work
DA imprinted PPy -ta-C/CNFs	0.01–1	DMEM/F-12, 15% HS and 2.5% FBS	53.26	This work

[a] : multi-walled carbon nanotubes spaced graphene aerogels (MWCNT/GAs),.
[b] : O-phenylenediamine,.
[c] : Poly thionine nanoporous gold,.
[d] : Poly(p-aminothiophenol),.
[e] : DA imprinted poly(5-amino 8-hydroxy quinoline) immobilized reduced graphene oxide.

neurons in vitro.

Supplementary data

Additional SEM images for ta-C/CNFs/MIP and comparison of electrochemical performance of different electrodes in presence of ISR and OSR probes.

CRediT authorship contribution statement

Khadijeh Nekoueian: Investigation, Conceptualization, Validation, Formal analysis, Visualization, Writing – original draft, Writing – review & editing. **Maedeh Akhoundian:** Formal analysis, Writing – review & editing. **Niklas Wester:** Formal analysis. **Tomi Laurila:** Supervision, Conceptualization, Writing – review & editing.

Declaration of Competing Interest

The authors declare that they have no known competing financial interests or personal relationships that could have appeared to influence the work reported in this paper.

Data availability

Data will be made available on request.

Acknowledgments

The authors acknowledge D.Sc. Sami Sainio for ta-C/CNFs samples. This work was supported by funding from the European Union's Horizon2020 research project number 68011531 CONNECT. The authors acknowledge the provision of facilities by the Aalto University Ota Nano−Micronova Nanofabrication Center, OtaNano−Nanomicroscopy Center (Aalto-NMC).

Supplementary materials

Supplementary material associated with this article can be found, in the online version, at doi:10.1016/j.electacta.2023.142029.

References

[1] S. Latif, et al., Dopamine in Parkinson's disease, Clin. Chim. Acta 522 (2021) 114–126, https://doi.org/10.1016/j.cca.2021.08.009.
[2] J. Kim, et al., Automatic and reliable quantification of tonic dopamine concentrations *in vivo* using a novel probabilistic inference method, ACS Omega 6 (10) (2021) 6607–6613, https://doi.org/10.1021/acsomega.0c05217. Mar.
[3] J.A. Johnson, N.T. Rodeberg, R.M. Wightman, Measurement of basal neurotransmitter levels using convolution-based nonfaradaic current removal, Anal. Chem. 90 (12) (2018) 7181–7189, https://doi.org/10.1021/acs.analchem.7b04682. Jun.
[4] I.M. Taylor, N.A. Patel, N.C. Freedman, E. Castagnola, X.T. Cui, Direct *in vivo* electrochemical detection of resting dopamine using poly(3,4-ethylenedioxythiophene)/carbon nanotube functionalized microelectrodes, Anal. Chem. 91 (20) (2019) 12917–12927, https://doi.org/10.1021/acs.analchem.9b02904. Oct.
[5] J.S. Cristóvão, B.J. Henriques, C.M. Gomes, Biophysical and spectroscopic methods for monitoring protein misfolding and amyloid aggregation. Protein Misfolding Diseases, Springer, 2019, pp. 3–18.
[6] D. Qi, et al., Quantification of dopamine in brain microdialysates with high-performance liquid chromatography–tandem mass spectrometry, Anal. Sci. 32 (4) (2016) 419–424.
[7] H. Rafi, A.G. Zestos, Review—recent advances in FSCV detection of neurochemicals via waveform and carbon microelectrode modification, J. Electrochem. Soc. 168 (5) (2021) 57520, https://doi.org/10.1149/1945-7111/ac0064.
[8] B. Bucur, C. Purcarea, S. Andreescu, A. Vasilescu, Addressing the selectivity of enzyme biosensors: solutions and perspectives, Sensors 21 (9) (2021), https://doi.org/10.3390/s21093038.
[9] E.N. Zare, et al., Electroconductive multi-functional polypyrrole composites for biomedical applications, Appl. Mater. Today 24 (2021), 101117, https://doi.org/10.1016/j.apmt.2021.101117.
[10] A. Manzari-Tavakoli, R. Tarasi, R. Sedghi, A. Moghimi, H. Niknejad, Fabrication of nanochitosan incorporated polypyrrole/alginate conducting scaffold for neural

tissue engineering, Sci. Rep. 10 (1) (2020) 22012, https://doi.org/10.1038/s41598-020-78650-2.
[11] S. Rantataro, et al., Nanoscale geometry determines mechanical biocompatibility of vertically aligned nanofibers, Acta Biomater. 146 (2022) 235–247, https://doi.org/10.1016/j.actbio.2022.04.032.
[12] C.C. Harley, V. Annibaldi, T. Yu, C.B. Breslin, The selective electrochemical sensing of dopamine at a polypyrrole film doped with an anionic β−cyclodextrin, J. Electroanal. Chem. 855 (2019), 113614, https://doi.org/10.1016/j.jelechem.2019.113614.
[13] G. Eom, et al., Highly sensitive and selective detection of dopamine using overoxidized polypyrrole/sodium dodecyl sulfate-modified carbon nanotube electrodes, J. Electroanal. Chem. 848 (2019), 113295, https://doi.org/10.1016/j.jelechem.2019.113295.
[14] D. Novosad, M. Hrenakova, J. Vacek, J. Storch, J. Styskala, J. Hrbac, Cyclopentenedione-based ascorbate-rejecting permselective layers prepared by electropolymerization, J. Electroanal. Chem. 912 (2022), 116261, https://doi.org/10.1016/j.jelechem.2022.116261.
[15] P.M. Tchekwagep, et al., A critical review on the use of molecular imprinting for trace heavy metal and micropollutant detection, Chemosensors 10 (8) (2022), https://doi.org/10.3390/chemosensors10080296.
[16] A.J. Kadhem, G.J. Gentile, M.M. Fidalgo de Cortalezzi, Molecularly imprinted polymers (MIPs) in sensors for environmental and biomedical applications: a review, Molecules 26 (20) (2021), https://doi.org/10.3390/molecules26206233.
[17] T. Kajisa, W. Li, T. Michinobu, T. Sakata, Well-designed dopamine-imprinted polymer interface for selective and quantitative dopamine detection among catecholamines using a potentiometric biosensor, Biosens. Bioelectron. 117 (2018) 810–817, https://doi.org/10.1016/j.bios.2018.07.014.
[18] Y. Mao, Y. Bao, S. Gan, F. Li, L. Niu, Electrochemical sensor for dopamine based on a novel graphene-molecular imprinted polymers composite recognition element, Biosens. Bioelectron. 28 (1) (2011) 291–297, https://doi.org/10.1016/j.bios.2011.07.034.
[19] N. Maouche, M. Guergouri, S. Gam-Derouich, M. Jouini, B. Nessark, M.M. Chehimi, Molecularly imprinted polypyrrole films: some key parameters for electrochemical picomolar detection of dopamine, J. Electroanal. Chem. 685 (2012) 21–27, https://doi.org/10.1016/j.jelechem.2012.08.020.
[20] Y. Li, et al., Fabrication of ultra-sensitive and selective dopamine electrochemical sensor based on molecularly imprinted polymer modified graphene@carbon nanotube foam, Electrochem. Commun. 64 (2016) 42–45, https://doi.org/10.1016/j.elecom.2016.01.009.
[21] F. Wang, L. Zhu, J. Zhang, Electrochemical sensor for levofloxacin based on molecularly imprinted polypyrrole–graphene–gold nanoparticles modified electrode, Sens. Actuators B Chem. 192 (2014) 642–647, https://doi.org/10.1016/j.snb.2013.11.037.
[22] J. Yang, Y. Hu, Y. Li, Molecularly imprinted polymer-decorated signal on-off ratiometric electrochemical sensor for selective and robust dopamine detection, Biosens. Bioelectron. 135 (2019) 224–230, https://doi.org/10.1016/j.bios.2019.03.054.
[23] L. Yang, F. Zhao, B. Zeng, Electrochemical determination of eugenol using a three-dimensional molecularly imprinted poly (p-aminothiophenol-co-p-aminobenzoic acids) film modified electrode, Electrochim. Acta 210 (2016) 293–300, https://doi.org/10.1016/j.electacta.2016.05.167.
[24] S. Kim, L.K. Jang, M. Jang, S. Lee, J.G. Hardy, J.Y. Lee, Electrically conductive polydopamine–polypyrrole as high performance biomaterials for cell stimulation *in vitro* and electrical signal recording *in vivo*, ACS Appl. Mater. Interfaces 10 (39) (2018) 33032–33042, https://doi.org/10.1021/acsami.8b11546. Oct.
[25] M. Meyyappan, Nano biosensors for neurochemical monitoring, Nano Converg. 2 (1) (2015) 18, https://doi.org/10.1186/s40580-015-0049-3.
[26] T. Qian, et al., Ultrasensitive dopamine sensor based on novel molecularly imprinted polypyrrole coated carbon nanotubes, Biosens. Bioelectron. 58 (2014) 237–241, https://doi.org/10.1016/j.bios.2014.02.081.
[27] X. Bai, B. Zhang, M. Liu, X. Hu, G. Fang, S. Wang, Molecularly imprinted electrochemical sensor based on polypyrrole/dopamine@graphene incorporated with surface molecularly imprinted polymers thin film for recognition of olaquindox, Bioelectrochemistry 132 (2020), 107398, https://doi.org/10.1016/j.bioelechem.2019.107398.
[28] X. Ma, et al., Novel electrochemical sensing platform based on a molecularly imprinted polymer-decorated 3D-multi-walled carbon nanotube intercalated graphene aerogel for selective and sensitive detection of dopamine, Anal. Methods 12 (14) (2020) 1845–1851, https://doi.org/10.1039/D0AY00033G.
[29] V.M.A. Mohanan, A.K. Kunnummal, V.M.N. Biju, Selective electrochemical detection of dopamine based on molecularly imprinted poly(5-amino 8-hydroxy quinoline) immobilized reduced graphene oxide, J. Mater. Sci. 53 (15) (2018) 10627–10639, https://doi.org/10.1007/s10853-018-2355-8.
[30] S. Sainio, et al., Structural morphology of carbon nanofibers grown on different substrates, Carbon N Y 98 (2016) 343–351, https://doi.org/10.1016/j.carbon.2015.11.021.
[31] S. Sainio, et al., Integrated carbon nanostructures for detection of neurotransmitters, Mol. Neurobiol. 52 (2) (2015) 859–866, https://doi.org/10.1007/s12035-015-9233-z.
[32] A. Kousar, E. Peltola, T. Laurila, Nanostructured geometries strongly affect fouling of carbon electrodes, ACS Omega 6 (40) (2021) 26391–26403, https://doi.org/10.1021/acsomega.1c03666. Oct.
[33] T. Palomäki, et al., Unmodified and multi-walled carbon nanotube modified tetrahedral amorphous carbon (ta-C) films as *in vivo* sensor materials for sensitive and selective detection of dopamine, Biosens. Bioelectron. 118 (2018) 23–30, https://doi.org/10.1016/j.bios.2018.07.018.
[34] T. Laurila, S. Sainio, M.A. Caro, Hybrid carbon based nanomaterials for electrochemical detection of biomolecules, Prog. Mater. Sci. 88 (2017) 499–594, https://doi.org/10.1016/j.pmatsci.2017.04.012.
[35] Y. Liu, K. Ai, L. Lu, Polydopamine and its derivative materials: synthesis and promising applications in energy, environmental, and biomedical fields, Chem. Rev. 114 (9) (2014) 5057–5115, https://doi.org/10.1021/cr400407a. May.
[36] T.P. Chen, T. Liu, T.L. Su, J. Liang, Self-polymerization of dopamine in acidic environments without oxygen, Langmuir 33 (23) (Jun. 2017) 5863–5871, https://doi.org/10.1021/acs.langmuir.7b01127.
[37] T. Palomäki, et al., Electron transport determines the electrochemical properties of tetrahedral amorphous carbon (ta-C) thin films, Electrochim. Acta 225 (2017) 1–10, https://doi.org/10.1016/j.electacta.2016.12.099.
[38] Y. Liu, J. Ma, T. Lu, L. Pan, Electrospun carbon nanofibers reinforced 3D porous carbon polyhedra network derived from metal-organic frameworks for capacitive deionization, Sci. Rep. 6 (1) (2016) 32784, https://doi.org/10.1038/srep32784.
[39] E. Leppänen, M. Akhoundian, S. Sainio, J. Etula, O. Pitkänen, T. Laurila, Structure-property relationships in carbon electrochemistry, Carbon N Y 200 (2022) 375–389, https://doi.org/10.1016/j.carbon.2022.08.076.
[40] R.L. McCreery, Advanced carbon electrode materials for molecular electrochemistry, Chem. Rev. 108 (7) (2008) 2646–2687, https://doi.org/10.1021/cr068076m. Jul.
[41] Y.S. Sung, L.Y. Lin, Systematic design of polypyrrole/carbon fiber electrodes for efficient flexible fiber-type solid-state supercapacitors, Nanomaterials 10 (2) (2020), https://doi.org/10.3390/nano10020248.
[42] B. Si, E. Song, Molecularly imprinted polymers for the selective detection of multi-analyte neurotransmitters, Microelectron. Eng. 187-188 (2018) 58–65, https://doi.org/10.1016/j.mee.2017.11.016.
[43] N. Ermiş, N. Tinkiliç, Development of an electrochemical sensor for selective determination of dopamine based on molecularly imprinted poly(p-aminothiophenol) polymeric film, Electroanalysis 33 (6) (2021) 1491–1501, https://doi.org/10.1002/elan.202060556. Jun.